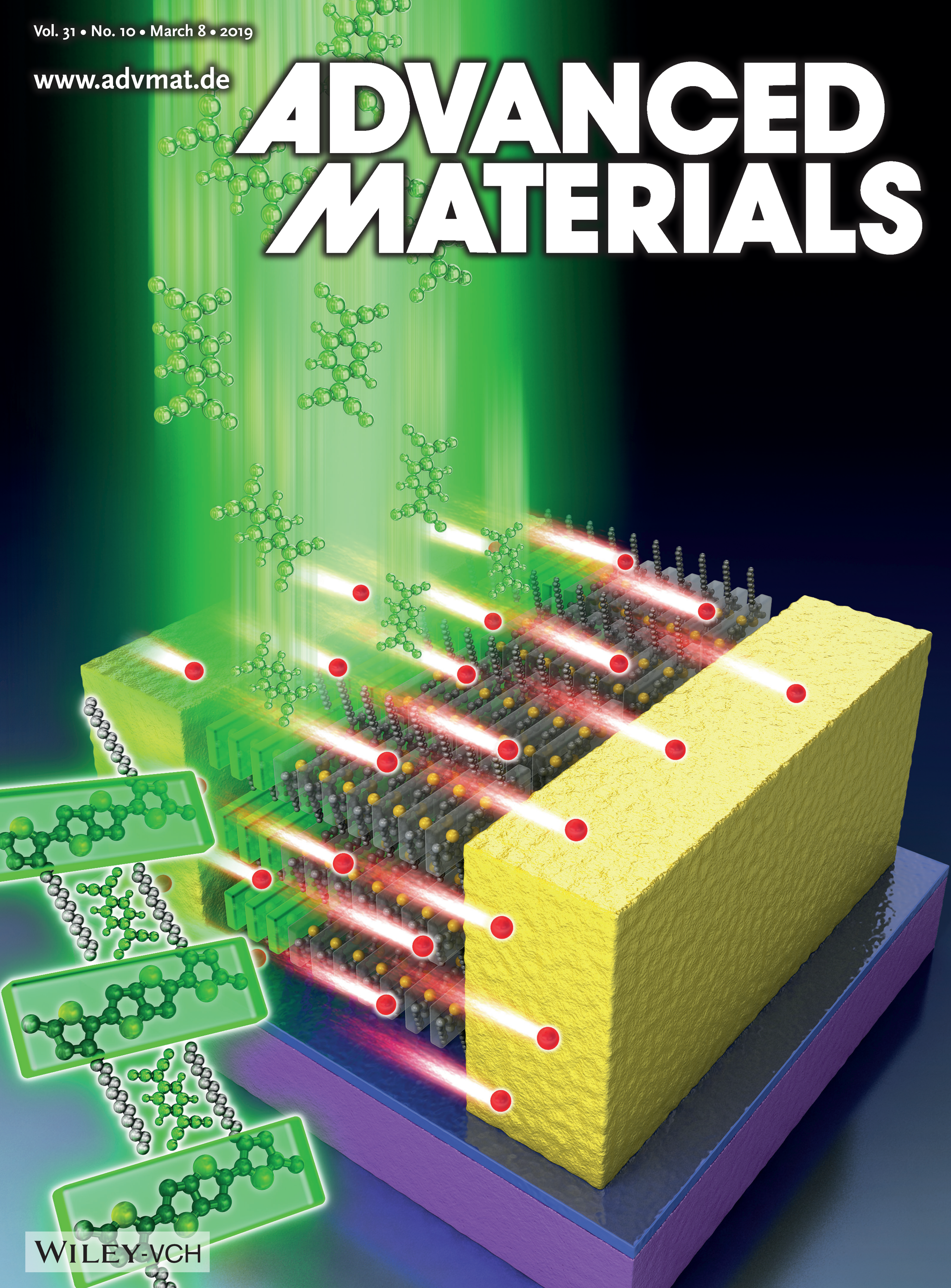
Vol. 31 • No. 10 • March 8 • 2019
www.advmat.de
ADVANCED MATERIALS
WILEY-VCH

ADVANCED MATERIALS
www.advmat.de

Enhanced Charge Injection Properties of Organic Field-Effect Transistor by Molecular Implantation Doping

Youngrok Kim, Seungjun Chung, Kyungjune Cho, David Harkin, Wang-Taek Hwang, Daekyoung Yoo, Jae-Keun Kim, Woocheol Lee, Younggul Song, Heebeom Ahn, Yongtaek Hong, Henning Sirringhaus, Keehoon Kang, and Takhee Lee**

Organic semiconductors (OSCs) have been widely studied due to their merits such as mechanical flexibility, solution processability, and large-area fabrication. However, OSC devices still have to overcome contact resistance issues for better performances. Because of the Schottky contact at the metal–OSC interfaces, a non-ideal transfer curve feature often appears in the low-drain voltage region. To improve the contact properties of OSCs, there have been several methods reported, including interface treatment by self-assembled monolayers and introducing charge injection layers. Here, a selective contact doping of 2,3,5,6-tetrafluoro-7,7,8,8-tetracyanoquinodimethane (F_4-TCNQ) by solid-state diffusion in poly(2,5-bis(3-hexadecylthiophen-2-yl)thieno[3,2-b]thiophene) (PBTTT) to enhance carrier injection in bottom-gate PBTTT organic field-effect transistors (OFETs) is demonstrated. Furthermore, the effect of post-doping treatment on diffusion of F_4-TCNQ molecules in order to improve the device stability is investigated. In addition, the application of the doping technique to the low-voltage operation of PBTTT OFETs with high-*k* gate dielectrics demonstrated a potential for designing scalable and low-power organic devices by utilizing doping of conjugated polymers.

Organic semiconductors (OSCs), widely applied as electronic devices such as organic light-emitting diodes, solar cells, memories, and organic field-effect transistors (OFETs), have various advantages including mechanical flexibility, low cost, solution-processed fabrication, and tunable material functionalities by molecular design compared with silicon-based materials.[1–13] However, the contact resistance problem arising between organic materials and metal electrodes has been one of the dominant obstacles for adopting organic semiconducting devices instead of silicon-based devices. Diverse attempts, for instance, self-assembled monolayer (SAM) treatment on metal electrodes,[14–19] inserting a charge injection layer between OSC and metals,[20–27] choice of metals for better injection properties,[28,29] adopting carbon-based conductor like graphene as electrodes,[30] have been introduced to improve carrier injection across typically a non-ohmic contact. Especially, considering large operation voltages required for OFETs, improving contact properties of organic/metal interface is an essential step for practical applications of OSCs.

Contact doping is one of the most effective techniques to reduce contact resistance and has been widely employed in silicon-based devices and recently in OSCs to reduce the contact resistance.[31–36] In order to avoid undesirable OFF currents, it needs to be performed selectively, i.e., in localized regions at the source–drain contacts only and not in the channel region. The doped regions have been usually confined to the top surface of the OSC film by depositing a small amount of dopants on the top of the organic film by thermal evaporation. As a result, the position of the gate dielectrics was normally restricted to the top side of devices (i.e., FETs in a top-gate structure) in order to enhance the charge injection from metal electrodes to the accumulation layer formed on the top surface of the polymer.[31,32] Recently, the combination of poly(2,5-bis(3-tetradecylthiophen-2-yl)thieno[3,2-b]thiophene) (PBTTT) and 2,3,5,6-tetrafluoro-7,7,8,8-tetracyanoquinodimethane (F_4-TCNQ) as host and dopant material, respectively, has produced a highly conducting polymer that has been studied as a candidate for a synthetic metal and high power-factor thermoelectric material.[37–41] Interestingly, this combination achieved an efficient bulk-doping of PBTTT by solid-state diffusion which implied that the F_4-TCNQ

Y. Kim, K. Cho, W.-T. Hwang, D. Yoo, J.-K. Kim, W. Lee, Dr. Y. Song, H. Ahn, Dr. K. Kang, Prof. T. Lee
Department of Physics and Astronomy, and Institute of Applied Physics
Seoul National University
Seoul 08826, Korea
E-mail: keehoon.kang@snu.ac.kr; tlee@snu.ac.kr

Dr. S. Chung
Photo-Electronic Hybrids Research Center
Korea Institute of Science and Technology
Seoul 02792, Korea

Dr. D. Harkin, Prof. H. Sirringhaus
Cavendish Laboratory
University of Cambridge
J. J. Thomson Avenue, Cambridge 0HE, UK

Prof. Y. Hong
Department of Electrical and Computer Engineering
Inter-University Semiconductor Research Center
Seoul National University
Seoul 08826, Korea

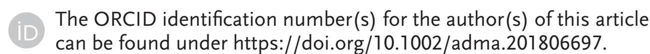
The ORCID identification number(s) for the author(s) of this article can be found under https://doi.org/10.1002/adma.201806697.

DOI: 10.1002/adma.201806697

 © 2019 WILEY-VCH Verlag GmbH & Co. KGaA, Weinheim

dopant molecules diffused into the PBTTT film all the way down to the interface between the PBTTT film and the SiO_2/Si substrate.[39] Moreover, the PBTTT film doped by solid-state diffusion exhibits a high conductivity of around 200 S cm^{-1} which would be applicable for selective contact doping for FETs.

One of the main challenges in utilizing selective molecular doping in organic optoelectronic devices has been the diffusion problem of dopant molecules in the host materials, which has reduced the device stability.[42–47] The dopant diffusion will especially be significant if one adopts selective bulk-doping on the contact regions of OFETs due to a large dopant concentration gradient of dopant molecules between the doped regions and active channel (non-doped) regions. To this date, there have been a relatively small number of studies that have directly investigated the diffusion problems within the selectively contact-doped OFETs.[32] In our study, the bulk-doping technique of PBTTT by solid-state diffusion of F_4-TCNQ was employed to provide highly conducting paths in order to enhance the charge injection in PBTTT OFETs in a bottom-gate structure. This technique is akin to an ion implantation doping technique employed in the silicon industry, hence the name "molecular implantation doping." We investigated and further improved the stability of the PBTTT OFETs by characterizing the effect of post-doping treatments on the dopant diffusion into the active channel. Moreover, we demonstrated that introducing the molecular implantation doping technique to the PBTTT OFETs with high-*k* gate dielectrics enabled a low-voltage operation, with improved charge injection properties.

Figure 1a,b shows the fabrication process of PBTTT OFETs with F_4-TCNQ doping on the contact regions of the devices and molecular structures of the used materials, respectively. More detailed information on the fabrication process can be found in the Experimental Section. The prepared substrates with the patterned source and drain electrodes were immersed in an octyltrichlorosilane (OTS) solution to form the OTS-SAM on the SiO_2. The measured contact angle with a water droplet was changed from 65.4° to 97.9° after the OTS-SAM treatment, indicating a clear OTS-SAM formation on the SiO_2 surfaces (Figure S1, Supporting Information).[48] The PBTTT films were spin-coated on the substrate (on OTS-SAM-treated SiO_2 and on the contact electrodes) and showed clear terrace structures with 2 nm steps (Figure S1, Supporting Information).[48–51] Then, the dopant material, F_4-TCNQ, was thermally evaporated with a nominal thickness of 10 nm by shadow masks on the contact areas as depicted in Figure 1a. The dopant molecules diffuse into the PBTTT film, creating a decaying depth-profile of the dopant distribution, as directly shown from our previous work.[39] Therefore, it was crucial to optimize the amount of dopants so that we can still achieve a good conductivity at the regions near the contact electrodes to enhance charge injection, while suppressing the dopant diffusion near the top surface. The doped regions of the PBTTT film appear more transparent as shown in the marked regions with arrows in the middle image of Figure 1c. When the dopant deposition was finished, the surface of the PBTTT films was immediately etched by argon plasma for 1 s to minimize diffusion of the dopant which caused a rise of the off-current of the OFET (defined as the minimum current value during the gate bias sweeps). The etching process was done because we anticipated the diffusion of

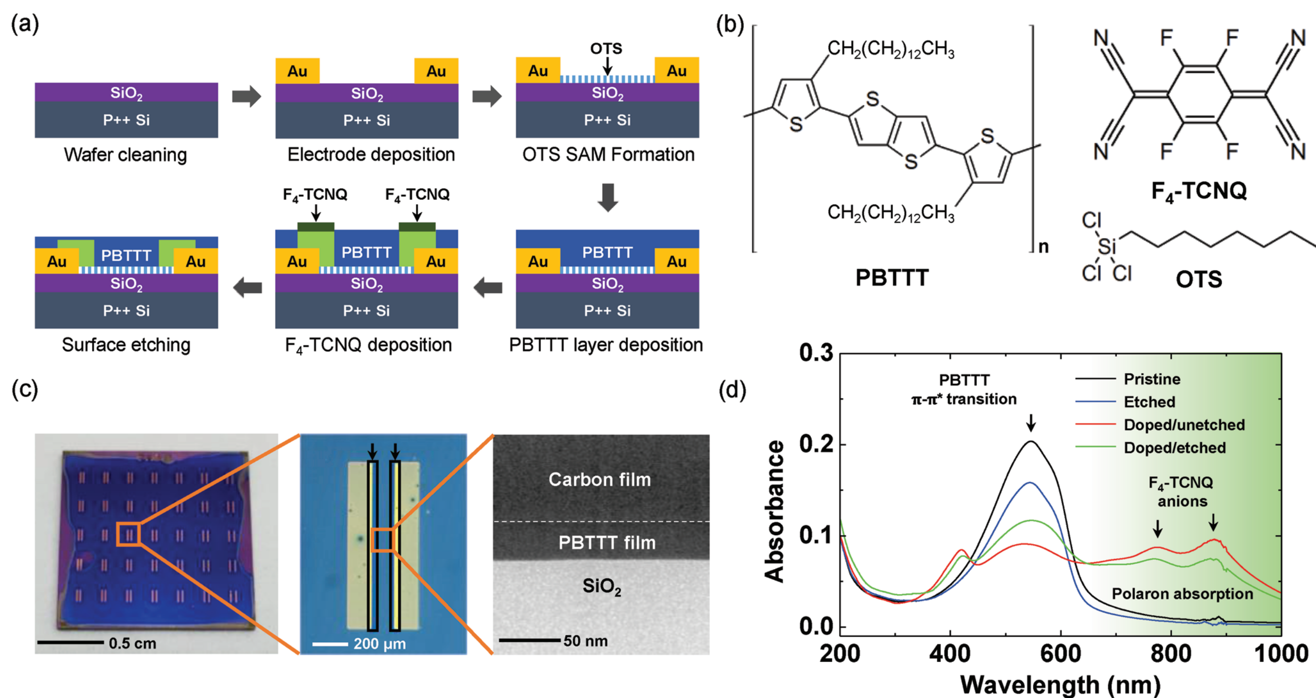

Figure 1. a) Schematic images of the device fabrication process. The dark green regions in the bottom-middle image represent neutral F_4-TCNQ molecules and the bright green regions in the last two steps represent the doped PBTTT. b) Molecular structures of PBTTT, F_4-TCNQ, and OTS. c) Optical images (left, middle) and a TEM image (right) of the selectively doped PBTTT transistors. The black rectangular areas (middle image) represent the doped regions of the PBTTT film. d) UV–vis spectra for pristine PBTTT, etched PBTTT, doped/unetched PBTTT, and doped/etched PBTTT films. The shaded area (in green) denotes a broad polaron absorption.

© 2019 WILEY-VCH Verlag GmbH & Co. KGaA, Weinheim

the dopant into the channel to be mainly caused by the neutral dopant molecules which did not undergo charge transfer with PBTTT. It was suggested from the previous research that the etching rate of F_4-TCNQ molecules was much faster than that of PBTTT and the neutral dopant molecules mainly remained near the surface of the PBTTT film.[39] Therefore, we inferred that the etching process reduced the neutral dopant concentration near the top surface of the doped regions of the PBTTT films. From the transmission electron microscopy (TEM) cross-sectional image (Figure 1c) and energy-dispersive spectrometer element analysis, we found that the thickness of the PBTTT film was ≈30 nm by tracing the sulfur signals (Figure S2, Supporting Information). Figure 1d shows an ultraviolet–visible (UV–vis) absorption data of various kinds of PBTTT films: a pristine (black line), etched (blue line), doped and unetched (denoted as "doped/unetched," red line), and doped and etched (denoted as "doped/etched," green line). Compared with the pristine film data, the etched film data show a decrease in the absorption over the entire range, while maintaining the surface morphology (Figure S3, Supporting Information). This implies that the PBTTT films were peeled off layer by layer by the etching. By controlling the amount of F_4-TCNQ dopant molecules with a nominal thickness of 10 nm, the data for both of the doped films show that the amount of the neutral dopants on the film was much less than the previous research with a small peak near 400 nm which is a unique absorption feature of the neutral F_4-TCNQ.[39] Furthermore, the data for both of the doped films show a clear bleaching of the π–π^* transition peak of PBTTT (resulting in a color change as seen from the middle image of Figure 1c) and the appearance of distinct peaks corresponding to F_4-TCNQ anion (near 780 and 890 nm). These results mean that the amount of the dopant molecules was considerably optimized, and therefore most of the dopant molecules diffuse into the PBTTT without leaving too much neutral dopants. The shaded area (in green) of this UV–vis plot indicates a broad polaron absorption in PBTTT, which indicates the generation of hole carriers in PBTTT via charge transfer.[52,53] The doped/etched film data show a slight recovery of the π–π^* transition peak of PBTTT, and a shrinkage of the neutral F_4-TCNQ and F_4-TCNQ anion peaks near 400 and 800 nm, respectively. These results imply that the etching caused a slight de-doping at the top surface of the doped PBTTT films by preferential etching of the dopant molecules (as shown in the final step of the fabrication process in Figure 1a).

Figure 2a shows the transfer curve of the transistor for both the linear and saturation regimes. The doped contact (i.e., doped/etched, donated as "DC") PBTTT transistors

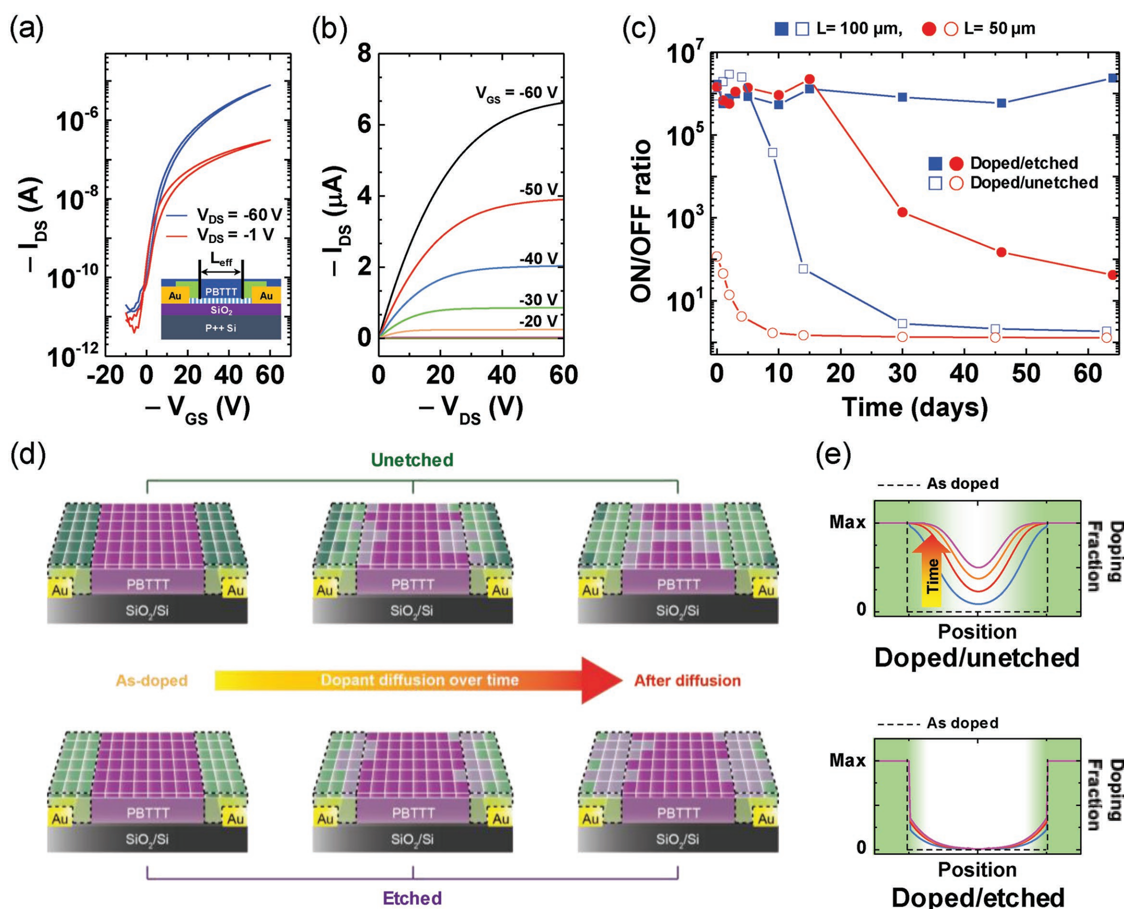

Figure 2. a) I_{DS}–V_{GS} transfer curves with a schematic image of the effective channel length (L_{eff}) and b) I_{DS}–V_{DS} output curves of a doped contact (doped/etched) PBTTT transistor. c) ON/OFF ratio stability for the doped PBTTT transistors with a channel length (L) of 50 and 100 μm. d) Schematic images of doped region propagation by the diffusion of neutral dopants. e) Simulation results of the doped region propagation with diffusion equation. The dashed lines denote the initial doping profile.

© 2019 WILEY-VCH Verlag GmbH & Co. KGaA, Weinheim

showed the ON/OFF ratio of over 10^5 with the mobility of 0.045 cm^2 V^{-1} s^{-1}. Since the high conductivity of doped PBTTT is around 200 S cm^{-1}, the contact doping process reduces the effective channel length (L_{eff}) of the doped contact transistors. Therefore, the device parameters, including mobility and contact resistance, were extracted with L_{eff}. The employed equations for extracting the mobility values are provided in Section 3 in the Supporting Information. Compared with the pristine devices with the mobility of 0.053 cm^2 V^{-1} s^{-1}, DC PBTTT transistors had a slightly lower mobility, which was caused by the etching process. This is supported by a slight decrease in the mobility of another reference pristine PBTTT OFET from 0.060 to 0.051 cm^2 V^{-1} s^{-1} after the etching process (see Section 3, Supporting Information). Although the surface morphology was not changed by the etching, the water contact angle of the PBTTT films was changed from 101.7° to 67.3°, which implies a slight change of chemical properties of the film surface (Figure S6, Supporting Information). Figure 2b shows the I_{DS}–V_{DS} output curves of DC transistors, which represent favorable output characteristics without the S-shape at a low V_{DS} regime that is typically induced by a significant contact resistance. From the Y-function method, the extracted value of the contact resistance of DC PBTTT transistors was found to be 5.1 kΩ cm^{-1} and that of the pristine device was found to be 24.5 kΩ cm^{-1} (for more details, see Section 4, Supporting Information). The contact resistance of DC PBTTT transistor had a comparable value to the lowest value that has been reported in the literature.[32,54]

The etching process was an essential step for reducing the amount of the dopants and improving the stability of the devices. Figure 2c shows the ON/OFF ratio of the doped PBTTT transistors either etched (filled symbols) or unetched (empty symbols), measured over the time scale of 2 months. For the doped transistors with the channel length of 50 µm, the doped/etched devices preserved its ON/OFF ratio over 10^5 for about 15 days, whereas it was difficult to define the ON/OFF ratio for the doped/unetched devices just after fabrication due to a large off-current. For the channel length of 100 µm, the doped/etched devices preserved its ON/OFF ratio for more than 2 months; however, the ON/OFF ratio of the doped/unetched devices dropped significantly after 15 days. The decrease of the ON/OFF ratio was mainly caused by orders of magnitude increase in the off-current (Figure S8, Supporting Information). Figure 2d shows a schematic diagram that depicts different propagation rates of the doped region in the doped/unetched and doped/etched devices over time based on optical images of the doped region propagation (Figure S9, Supporting Information). The different propagation rates mainly result from different diffusion rates of the neutral dopant molecules, which have been shown to be much more diffusive than ionized dopant molecules.[55,56] The figure represents the possible formation of percolated current paths between the source and drain electrodes (i.e., the doped regions from each side meet in the middle), which would result in the rise of the off-current. The diffusion of the neutral dopant molecules takes place in both the doped/unetched and doped/etched devices, but such diffusion effect is less significant for the doped/etched device due to a lower initial amount of the neutral dopants at the top surface of the PBTTT film. Therefore, percolation paths are much more difficult to form in the doped/etched device. This concept could be verified by a numerical simulation which has been applied to reveal the diffusion velocity of molecules in various systems.[57–59] In our case, we solved a modified Fick's diffusion equation by a numerical simulation that accounts for the capturing of diffusive neutral dopant molecules via charge transfer. Although the only input parameter that varied between the doped/unetched and doped/etched cases was the initial amount of the neutral dopants, the doping fraction profiles show clear contrasts between the two cases (Figure 2e). Especially, we found that the doping fraction at the center of the PBTTT film (i.e., an indicator for the formation of the percolated current paths) was negligible for the doped/etched case whereas the doping fraction gradually increased over time for the doped/unetched case (shown as a block arrow in Figure 2e). The detailed discussion of the numerical simulation is written in Section 6 of the Supporting Information. We also discovered that the surface diffusion of the neutral dopants would be prohibited further by introducing a dielectric layer on top of the doped/etched PBTTT film. The ON/OFF ratio of the DC PBTTT transistors encapsulated with a CYTOP (CTL-809M; Asahi Glass) layer on top showed a greater stability over time for the devices with 50 µm channel length, compared to the DC devices without any layers on top (see Figure S11, Supporting Information). This result would be an evidence that the neutral dopant molecules diffuse primarily along the surface. A detailed investigation of a microscopic mechanism for the surface interaction between the CYTOP molecules and neutral dopants is beyond the scope of this study.

To confirm the doping effect on the carrier injection properties directly, we fabricated homogeneously doped (i.e., the entire PBTTT area in a transistor is doped and etched; denoted as "entire-doped") PBTTT devices with the channel length of 2 µm by a conventional photolithography. **Figure 3**a shows the I_{DS}–V_{DS} data of an entire-doped device measured from 80 to 300 K. For this temperature range, the entire-doped device showed a clear ohmic behavior. This result implies that the charge injection occurred without an activation barrier. Since 2D charge transport properties in PBTTT have been previously demonstrated,[39,60,61] the thermionic emission equation for 2D semiconducting system, $I_{DS} = R^* T^{\frac{3}{2}} \exp[(-q/k_B T)(\phi - V_{DS}/\eta)]$, was employed to extract the activation energy of the contact between the doped PBTTT and gold electrodes, where R^*, φ, and η denote the Richardson coefficient, the effective activation energy, and ideality factor, respectively (Figure S12, Supporting Information). The extracted thermal activation energy had negative values, which implies that a dominant charge injection mechanism was not likely to be thermionic emission.

To construct the band diagram of the contact region of the devices, ultraviolet photoelectron spectroscopy (UPS) was conducted for both the pristine and doped/unetched PBTTT films. Here, we used the doped/unetched PBTTT film for UPS data since we assume that the PBTTT molecules at the bottom side of devices were free from etching. Figure 3b shows the UPS spectra for binding energies near the Fermi level and secondary-electron cutoff region. The Fermi levels of these samples were calibrated by the UPS data of 50 nm thick gold film and the value of the work function of gold was determined to be 4.52 eV (Figure S13, Supporting Information). This value is

 © 2019 WILEY-VCH Verlag GmbH & Co. KGaA, Weinheim

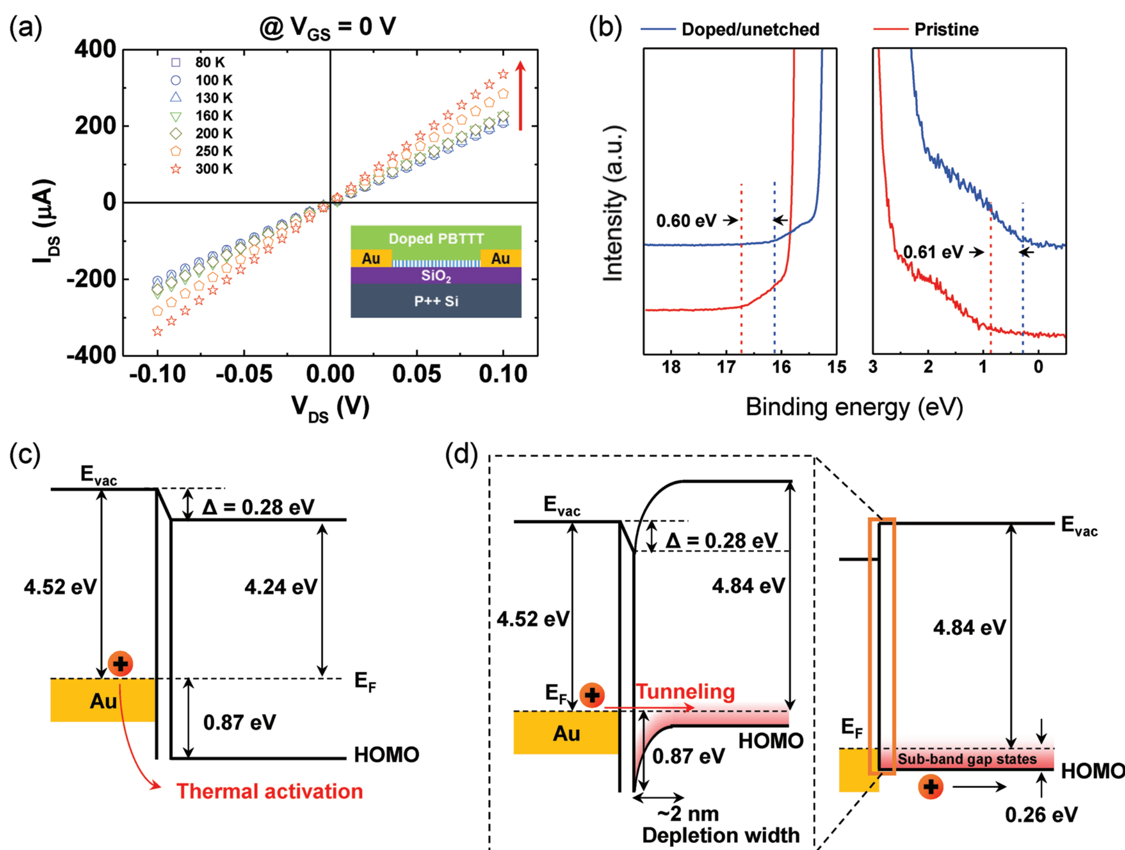

Figure 3. a) I_{DS}–V_{DS} output curves of an entire-doped PBTTT device at V_{GS} = 0 V in a temperature range from 80 to 300 K. b) The UPS data of the doped/unetched and pristine PBTTT films near the Fermi level (right) and secondary-electron cutoff (left). c,d) The band diagram near the contact of the pristine PBTTT transistor (c) and the doped contact PBTTT transistor, with a highlighted view of the band diagram at the contact (d).

slightly less than the typical 5.0 eV reported for gold presumably due to a low vacuum level (≈10^{-7} torr) used during the evaporation.[62,63] The UPS data showed similar shifts for both the highest occupied molecular orbital (HOMO) levels and secondary-electron cutoff levels of the PBTTT films after doping. The difference between the Fermi level and the HOMO level of the PBTTT film was reduced from 0.87 to 0.26 eV after doping. Figure 3c,d shows the band diagrams near the contact electrodes for the pristine and doped PBTTT molecules, based on the UPS analysis. We regarded that the interface dipole caused a vacuum level shift of 0.28 eV between the gold electrode and the PBTTT films.[64] Considering the charge concentration of the doped PBTTT film of about 3.3×10^{20} cm^{-3},[39] the depletion width between the doped PBTTT and gold is about 2 nm which is thin enough for tunneling.[35] From the I_{DS}–V_{DS} data of an entire-doped device and band diagram analysis, we considered that the charge injection of the devices was enhanced since the dominant charge injection mechanism was changed from thermionic emission (pristine transistors) to thermally assisted tunneling (doped contact transistors) via the doping of contact regions. Despite the 0.26 eV energy gap between the gold electrodes and the doped PBTTT molecules (Figure 3d), this contact showed ohmic properties as shown in Figure 3a. This may be due to sub-band gap states induced by doping which are accessible by injected charges from the electrodes via tunneling.

A crucial advantage of the bottom-gate structure employed in the study comes from its extra degree of freedom in the choice of the dielectric material that is compatible with the semiconductor. This is highly relevant for OFETs with high-k dielectric materials which typically require relatively high-temperature processes which result in irreversible damages to the OSC film, as well as exposure to chemical environments which can harm the OFET device performance (e.g., exposure to water during atomic layer deposition [ALD]).[65] Therefore, in order to use high-k dielectric materials for low-voltage operation of OFETs, the dielectric materials should be ideally deposited before the OSCs. To demonstrate the advantage of the molecular implantation doping in the low-voltage operation of OFETs, we adopted Al_2O_3 as the bottom gate dielectric deposited by ALD. **Figure 4**a illustrates the fabrication process of the high-k devices. A detailed fabrication process is described in the Supporting Information (Figure S14, Supporting Information). The TEM cross-sectional image in Figure 4a shows 25 nm thick Al_2O_3 and a 5 nm thick native SiO_2 on a silicon substrate. The measured capacitance value after the Al_2O_3 deposition was 2.36×10^{-7} F cm^{-2} (Figure S15, Supporting Information). This capacitance value is about 18 times higher than the capacitance value for the 270 nm thick SiO_2 (1.28×10^{-8} F cm^{-2}) used in Figures 1 and 2. The OTS-SAM treatment showed an excellent improvement of the interface like in the SiO_2 case in terms of the PBTTT film morphology which is critical to the PBTTT

 © 2019 WILEY-VCH Verlag GmbH & Co. KGaA, Weinheim

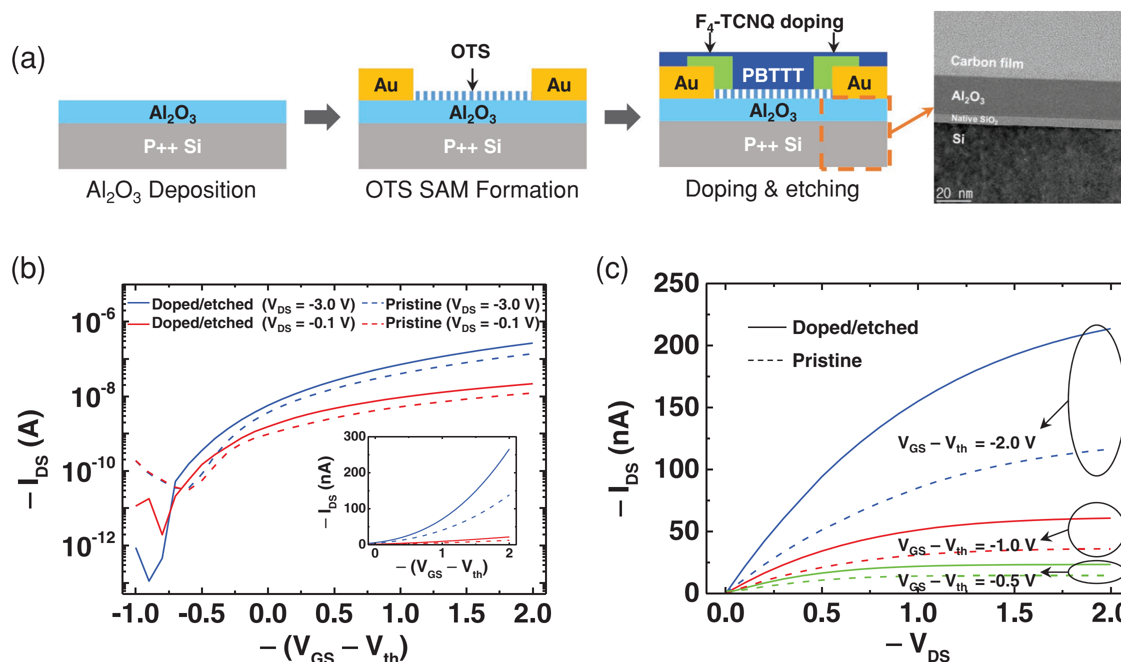

Figure 4. a) Schamtic images of the device fabrication process with a high-*k* dielectric. The rightmost figure shows the TEM cross-sectional image of Al_2O_3. b) I_{DS}–V_{GS} tranfer curves of the doped contact and pristine PBTTT transistors. Linear plots of the transfer curves are shown in the inset. c) I_{DS}–V_{DS} output curves of the doped contact and pristine PBTTT transistors.

OFET performance[66] (Figure S16, Supporting Information). As a result, the DC PBTTT transistors on Al_2O_3 had a similar mobility value to those on SiO_2. The transfer curves did not show a significant hysteresis which is usually induced by trap sites on the gate dielectric interface (Figure S17, Supporting Information). Figure 4b shows I_{DS}–V_{GS} transfer characteristics of the pristine and the DC PBTTT transistors on Al_2O_3 gate dielectrics with the channel length of 50 µm. All of the voltage biases were under 3 V to avoid dielectric breakdown.[67] The DC PBTTT device had about twice the value of I_{DS} value than the pristine one in both the linear and saturation regimes. Interestingly, these results indicate that the DC PBTTT devices had a larger mobility than the pristine devices: 0.037 $cm^2\ V^{-1}\ s^{-1}$ for DC PBTTT devices and 0.019 $cm^2\ V^{-1}\ s^{-1}$ for pristine devices. These results show that the reduction of the contact resistance is more effective in the low-voltage operation of the OFETs which could be applied to low power consumption organic electronics.

In conclusion, we have demonstrated an enhanced charge injection in PBTTT OFETs by molecular implantation doping with F_4-TCNQ and introduced an argon plasma etching treatment for improving the off-current stability. With this approach, the amount of neutral dopants was effectively controlled and the dopant diffusion into the active channel of the PBTTT OFETs was significantly suppressed. If the neutral dopants are removed completely by furthur optimization, this technique could work even for devices with smaller channel length. The low-temperature measurement and the band diagram analysis implied that the enhanced charge injection properties originated from the change of the dominant charge injection mechanism from thermionic emission to tunneling at the contact between the doped PBTTT films and metal electrodes. In addition, we demonstrated the low-voltage operation devices by using Al_2O_3 as a high-*k* gate dielectric material. For the high-*k* devices, the doped contact PBTTT transistor showed a better performance compared with the pristine devices. This study provides clear evidences that the molecular implantation doping is potentially one of the key techniques for solving the contact resistance issue for OFETs, thereby facilitating low-power oragnic electronics.

Experimental Section

SiO_2/p++ Si substrates were cleaned using de-ionized water, isopropanol, and acetone for 10 min in each cleaning solvent by sonication in an ultrasonic bath. Then, the source and drain electrodes of Ti/Au (2 nm/30 nm) were deposited with shadow masks on the substrates by using an electron-beam evaporator with a deposition rate of 0.5 Å s^{-1} at a pressure of ≈10^{-7} torr. After further cleaning with an oxygen plasma etching (50 W for 2 min), the substrates were transferred immediately to a nitrogen atmosphere glove box and were immersed in a prepared OTS solution (30 m M in anhydrous toluene) for ≈12 h. At the end of the OTS-SAM treatment, the substrates were cleaned in toluene, isopropanol, acetone, and toluene again by sonication for 10 min in each solvent and were stocked in a vacuum chamber for ≈2 h. The PBTTT solution was prepared in anhydrous 1,2-dichlorobenzene with a concentration of 9 mg mL^{-1}. Before spin-coating, the PBTTT solution was heated at 110 °C and the PBTTT films were spin-coated at 1500 rpm for 45 s in the N_2-filled glove box, followed by annealing at 180 °C, and then the films were cooled down to room temperature slowly. After the PBTTT film deposition, F_4-TCNQ dopant molecules were thermally evaporated directly onto the selected region of the PBTTT film with a nominal thickness of 10 nm by shadow masks with the rate of 0.5–1.5 Å s^{-1} at a pressure of ≈10^{-6} torr. After doping, the devices were etched immediately by argon plasma etching (50 W for 1 s).

© 2019 WILEY-VCH Verlag GmbH & Co. KGaA, Weinheim

Supporting Information

Supporting Information is available from the Wiley Online Library or from the author.

Acknowledgements

This work was supported by the National Creative Research Laboratory Program (grant No. 2012026372) through the National Research Foundation of Korea funded by the Korean Ministry of Science and ICT. S.C. appreciates the financial support from the Korean Ministry of Trade, Industry & Energy and Korea Display Research Consortium support program (10051541). Y.H. appreciates the financial support from the R&D Convergence Program of NST (National Research Council of Science & Technology) of Korea (CAP-15-04-KITECH). D.H. would like to thank the Doctoral Training Centre in Plastic Electronics EP/G037515/1. H.S. acknowledges funding from the European Research Council (ERC) through a Synergy Grant (Grant No. 610116). The authors thank R. D. Pietro for valuable discussions.

Conflict of Interest

The authors declare no conflict of interest.

Keywords

charge injection, doping, F_4-TCNQ, organic field-effect transistors, PBTTT, solid-state diffusion

Received: October 15, 2018
Revised: November 13, 2018
Published online: January 22, 2019

[1] X. Gu, L. Shaw, K. Gu, M. F. Toney, Z. Bao, *Nat. Commun.* **2018**, *9*, 534.
[2] W.-Y. Lee, H.-C. Wu, C. Lu, B. D. Naab, W.-C. Chen, Z. Bao, *Adv. Mater.* **2017**, *29*, 1605166.
[3] T. Someya, Z. Bao, G. G. Malliaras, *Nature* **2016**, *540*, 379.
[4] H. Sirringhaus, *Adv. Mater.* **2014**, *26*, 1319.
[5] M. Kaltenbrunner, T. Sekitani, J. Reeder, T. Yokota, K. Kuribara, T. Tokuhara, M. Drack, R. Schwödiauer, I. Graz, S. Bauer-Gogonea, S. Bauer, T. Someya, *Nature* **2013**, *499*, 458.
[6] H. Kang, R. Kitsomboonloha, J. Jang, V. Subramanian, *Adv. Mater.* **2012**, *24*, 3065.
[7] T. Sekitani, T. Someya, *Mater. Today* **2011**, *14*, 398.
[8] A. de la Fuente Vornbrock, D. Sung, H. Kang, R. Kitsomboonloha, V. Subramanian, *Org. Electron.* **2010**, *11*, 2037.
[9] T. Sekitani, H. Nakajima, H. Maeda, T. Fukushima, T. Aida, K. Hata, T. Someya, *Nat. Mater.* **2009**, *8*, 494.
[10] T. Sekitani, M. Takamiya, Y. Noguchi, S. Nakano, Y. Kato, T. Sakurai, T. Someya, *Nat. Mater.* **2007**, *6*, 413.
[11] Y.-Y. Noh, N. Zhao, M. Caironi, H. Sirringhaus, *Nat. Nanotechnol.* **2007**, *2*, 784.
[12] J. B. Lee, V. Subramanian, *IEEE Trans. Electron Devices* **2005**, *52*, 269.
[13] G. Yu, J. Gao, J. C. Hummelen, F. Wudl, A. J. Heeger, *Science* **1995**, *270*, 1789.
[14] J. Youn, G. R. Dholakia, H. Huang, J. W. Hennek, A. Facchetti, T. J. Marks, *Adv. Funct. Mater.* **2012**, *22*, 1856.
[15] K. A. Singh, T. L. Nelson, J. A. Belot, T. M. Young, N. R. Dhumal, T. Kowalewski, R. D. McCullough, P. Nachimuthu, S. Thevuthasan, L. M. Porter, *ACS Appl. Mater. Interfaces* **2011**, *3*, 2973.
[16] Y.-Y. Noh, X. Cheng, M. Tello, M.-J. Lee, H. Sirringhaus, *Semicond. Sci. Technol.* **2011**, *26*, 034003.
[17] D. Boudinet, M. Benwadih, Y. Qi, S. Altazin, J.-M. Verilhac, M. Kroger, C. Serbutoviez, R. Gwoziecki, R. Coppard, G. Le Blevennec, A. Kahn, G. Horowitz, *Org. Electron.* **2010**, *11*, 227.
[18] X. Cheng, Y.-Y. Noh, J. Wang, M. Tello, J. Frisch, R.-P. Blum, A. Vollmer, J. P. Rabe, N. Koch, H. Sirringhaus, *Adv. Funct. Mater.* **2009**, *19*, 2407.
[19] P. Marmont, N. Battaglini, P. Lang, G. Horowitz, J. Hwang, A. Kahn, C. Amato, P. Calas, *Org. Electron.* **2008**, *9*, 419.
[20] D. He, J. Qiao, L. Zhang, J. Wang, T. Lan, J. Qian, Y. Li, Y. Shi, Y. Chai, W. Lan, L. K. Ono, Y. Qi, J.-B. Xu, W. Ji, X. Wang, *Sci. Adv.* **2017**, *3*, e1701186.
[21] C. G. Tang, M. C. Y. Ang, K.-K. Choo, V. Keerthi, J.-K. Tan, M. N. Syafiqah, T. Kugler, J. H. Burroughes, R.-Q. Png, L.-L. Chua, P. K. H. Ho, *Nature* **2016**, *539*, 536.
[22] S. Chung, M. Jang, S.-B. Ji, H. Im, N. Seong, J. Ha, S.-K. Kwon, Y.-H. Kim, H. Yang, Y. Hong, *Adv. Mater.* **2013**, *25*, 4773.
[23] Y. Zhou, C. Fuentes-Hernandez, J. Shim, J. Meyer, A. J. Giordano, H. Li, P. Winget, T. Papadopoulos, H. Cheun, J. Kim, M. Fenoll, A. Dindar, W. Haske, E. Najafabadi, T. M. Khan, H. Sojoudi, S. Barlow, S. Graham, J.-L. Brédas, S. R. Marder, A. Kahn, B. Kippelen, *Science* **2012**, *336*, 327.
[24] T. Minari, P. Darmawan, C. Liu, Y. Li, Y. Xu, K. Tsukagoshi, *Appl. Phys. Lett.* **2012**, *100*, 093303.
[25] M. Kröger, S. Hamwi, J. Meyer, T. Riedl, W. Kowalsky, A. Kahn, *Appl. Phys. Lett.* **2009**, *95*, 123301.
[26] M. Kano, T. Minari, K. Tsukagoshi, *Appl. Phys. Lett.* **2009**, *94*, 143304.
[27] S. Cho, J. H. Seo, K. Lee, A. J. Heeger, *Adv. Funct. Mater.* **2009**, *19*, 1459.
[28] B. H. Hamadani, D. J. Gundlach, I. McCulloch, M. Heeney, *Appl. Phys. Lett.* **2007**, *91*, 243512.
[29] D. J. Gundlach, L. Zhou, J. A. Nichols, T. N. Jackson, P. V. Necliudov, M. S. Shur, *J. Appl. Phys.* **2006**, *100*, 024509.
[30] S. Lee, G. Jo, S.-J. Kang, G. Wang, M. Choe, W. Park, D.-Y. Kim, Y. H. Kahng, T. Lee, *Adv. Mater.* **2011**, *23*, 100.
[31] Y. Xu, H. Sun, W. Li, Y.-F. Lin, F. Balestra, G. Ghibaudo, Y.-Y. Noh, *Adv. Mater.* **2017**, *29*, 1702729.
[32] Y. Xu, H. Sun, E.-Y. Shin, Y.-F. Lin, W. Li, Y.-Y. Noh, *Adv. Mater.* **2016**, *28*, 8531.
[33] B. Lüssem, C.-M. Keum, D. Kasemann, B. Naab, Z. Bao, K. Leo, *Chem. Rev.* **2016**, *116*, 13714.
[34] A. A. Günther, M. Sawatzki, P. Formánek, D. Kasemann, K. Leo, *Adv. Funct. Mater.* **2016**, *26*, 768.
[35] D. Khim, K.-J. Baeg, M. Caironi, C. Liu, Y. Xu, D.-Y. Kim, Y.-Y. Noh, *Adv. Funct. Mater.* **2014**, *24*, 6252.
[36] S. Singh, S. K. Mohapatra, A. Sharma, C. Fuentes-Hernandez, S. Barlow, S. R. Marder, B. Kippelen, *Appl. Phys. Lett.* **2013**, *102*, 153303.
[37] D. T. Duong, Y. Tuchman, P. Chakthranont, P. Cavassin, R. Colucci, T. F. Jaramillo, A. Salleo, G. C. Faria, *Adv. Electron. Mater.* **2018**, *4*, 1800090.
[38] S. N. Patel, A. M. Glaudell, K. A. Peterson, E. M. Thomas, K. A. O'Hara, E. Lim, M. L. Chabinyc, *Sci. Adv.* **2017**, *3*, e1700434.
[39] K. Kang, S. Watanabe, K. Broch, A. Sepe, A. Brown, I. Nasrallah, M. Nikolka, Z. Fei, M. Heeney, D. Matsumoto, K. Marumoto, H. Tanaka, S.-i. Kuroda, H. Sirringhaus, *Nat. Mater.* **2016**, *15*, 896.
[40] A. M. Glaudell, J. E. Cochran, S. N. Patel, M. L. Chabinyc, *Adv. Energy Mater.* **2015**, *5*, 1401072.

© 2019 WILEY-VCH Verlag GmbH & Co. KGaA, Weinheim

[41] J. E. Cochran, M. J. N. Junk, A. M. Glaudell, P. L. Miller, J. S. Cowart, M. F. Toney, C. J. Hawker, B. F. Chmelka, M. L. Chabinyc, *Macromolecules* **2014**, *47*, 6836.
[42] J. Li, C. W. Rochester, I. E. Jacobs, S. Friedrich, P. Stroeve, M. Riede, A. J. Moulé, *ACS Appl. Mater. Interfaces* **2015**, *7*, 28420.
[43] A. Dai, A. Wan, C. Magee, Y. Zhang, S. Barlow, S. R. Marder, A. Kahn, *Org. Electron.* **2015**, *23*, 151.
[44] B. Lüssem, M. Riede, K. Leo, *Phys. Status Solidi A* **2013**, *210*, 9.
[45] I. Bruder, S. Watanabe, J. Qu, I. B. Müller, R. Kopecek, J. Hwang, J. Weis, N. Langer, *Org. Electron.* **2010**, *11*, 589.
[46] W. Gao, A. Kahn, *Org. Electron.* **2002**, *3*, 53.
[47] W. Gao, A. Kahn, *Appl. Phys. Lett.* **2001**, *79*, 4040.
[48] T. Umeda, S. Tokito, D. Kumaki, *J. Appl. Phys.* **2007**, *101*, 054517.
[49] S. Himmelberger, J. Dacuña, J. Rivnay, L. H. Jimison, T. McCarthy-Ward, M. Heeney, I. McCulloch, M. F. Toney, A. Salleo, *Adv. Funct. Mater.* **2013**, *23*, 2091.
[50] C. Wang, L. H. Jimison, L. Goris, I. McCulloch, M. Heeney, A. Ziegler, A. Salleo, *Adv. Mater.* **2010**, *22*, 697.
[51] I. McCulloch, M. Heeney, C. Bailey, K. Genevicius, I. MacDonald, M. Shkunov, D. Sparrowe, S. Tierney, R. Wagner, W. Zhang, M. L. Chabinyc, R. J. Kline, M. D. McGehee, M. F. Toney, *Nat. Mater.* **2006**, *5*, 328.
[52] M. C. Gwinner, R. D. Pietro, Y. Vaynzof, K. J. Greenberg, P. K. H. Ho, R. H. Friend, H. Sirringhaus, *Adv. Funct. Mater.* **2011**, *21*, 1432.
[53] N. Zhao, Y.-Y. Noh, J.-F. Chang, M. Heeney, I. McCulloch, H. Sirringhaus, *Adv. Mater.* **2009**, *21*, 3759.
[54] T. Umeda, D. Kumaki, S. Tokito, *J. Appl. Phys.* **2009**, *105*, 024516.
[55] J. Li, C. Koshnick, S. O. Diallo, S. Ackling, D. M. Huang, I. E. Jacobs, T. F. Harrelson, K. Hong, G. Zhang, J. Beckett, M. Mascal, A. J. Moule, *Macromolecules* **2017**, *50*, 5476.
[56] P. Reiser, L. Müller, V. Sivanesan, R. Lovrincic, S. Barlow, S. R. Marder, A. Pucci, W. Jaegermann, E. Mankel, S. Beck, *J. Phys. Chem. C* **2018**, *122*, 14518.
[57] Y. Cheng, G. Zhang, Y. Zhang, T. Chang, Q.-X. Pei, Y. Cai, Y.-W. Zhang, *Nanoscale* **2018**, *10*, 1660.
[58] P. A. Stolk, H.-J. Gossmann, D. J. Eaglesham, D. C. Jacobson, C. S. Rafferty, G. H. Gilmer, M. Jaraíz, J. M. Poate, H. S. Luftman, T. E. Haynes, *J. Appl. Phys.* **1997**, *81*, 6031.
[59] P. M. Fahey, P. B. Griffin, J. D. Plummer, *Rev. Mod. Phys.* **1989**, *61*, 289.
[60] K. Cho, J. Pak, J.-K. Kim, K. Kang, T.-Y. Kim, J. Shin, B. Y. Choi, S. Chung, T. Lee, *Adv. Mater.* **2018**, *30*, 1705540.
[61] A. J. Kronemeijer, V. Pecunia, D. Venkateshvaran, M. Nikolka, A. Sadhanala, J. Moriarty, M. Szumilo, H. Sirringhaus, *Adv. Mater.* **2014**, *26*, 728.
[62] M. Fahlman, A. Crispin, X. Crispin, S. K. M. Henze, M. P. de Jong, W. Osikowicz, C. Tengstedt, W. R. Salaneck, *J. Phys.: Condens. Matter* **2007**, *19*, 183202.
[63] W. Osikowicz, M. P. de Jong, S. Braun, C. Tengstedt, M. Fahlman, W. R. Salaneck, *Appl. Phys. Lett.* **2006**, *88*, 193504.
[64] S. Olthof, W. Tress, R. Meerheim, B. Lüssem, K. Leo, *J. Appl. Phys.* **2009**, *106*, 103711.
[65] M. Leskelä, M. Ritala, *Thin Solid Films* **2002**, *409*, 138.
[66] M. J. Lee, D. Gupta, N. Zhao, M. Heeney, I. McCulloch, H. Sirringhaus, *Adv. Funct. Mater.* **2011**, *21*, 932.
[67] Y. Wu, B. Lee, H.-S. P. Wong, *IEEE Electron Device Lett.* **2010**, *31*, 1449.

 © 2019 WILEY-VCH Verlag GmbH & Co. KGaA, Weinheim